IEEE Open Journal of
Industry Applications

Received 23 February 2024; revised 30 April 2024 and 18 June 2024; accepted 8 July 2024. Date of publication 10 July 2024; date of current version 22 July 2024. The review of this article was arranged by Associate Editor Erika Stracqualursi.

Digital Object Identifier 10.1109/OJIA.2024.3426334

Fast Transient Stability Assessment of Power Systems Using Optimized Temporal Convolutional Networks

MOHAMED MASSAOUDI [1,2] (Member, IEEE), TASSNEEM ZAMZAM [1,2], MAYMOUNA EZ EDDIN [1,2], ALI GHRAYEB [2,3] (Fellow, IEEE), HAITHAM ABU-RUB [2,3] (Fellow, IEEE), AND SHADY S. REFAAT [4] (Senior Member, IEEE)

[1]Department of Electrical Engineering, Texas A&M University, College Station, TX 77840 USA
[2]Department of Electrical Engineering, Texas A&M University Qatar, Doha 23874, Qatar
[3]College of Science and Engineering, Hamad Bin Khalifa University, Doha 34110, Qatar
[4]School of Physics, Engineering, and Computer Science, University of Hertfordshire, AL10 9AB Hatfield, U.K.

CORRESPONDING AUTHOR: MOHAMED MASSAOUDI (e-mail: mohamed.massaoudi@qatar.tamu.edu)

This work was supported in part by the Qatar National Research Fund (QNRF is a member of Qatar Foundation) under Grant NPRP12C-33905-SP-213 and Grant NPRP12C-33905-SP-220, and in part by Qatar National Library through open access.

ABSTRACT The transient power grid stability is greatly affected by the unpredictability of inverter-based resources of today's interconnected power grids. This article introduces an efficient transient stability status prediction method based on deep temporal convolutional networks (TCNs). A grey wolf optimizer (GWO) is utilized to fine-tune the TCN hyperparameters to improve the proposed model's accuracy. The proposed model provides critical information on the transient grid status in the early stages of fault occurrence, which may lead to taking the proper action. The proposed TCN-GWO uses both synchronously sampled values and synthetic values from various bus systems. In a postfault scenario, a copula of processing blocks is implemented to ensure the reliability of the proposed method where high-importance features are incorporated into the TCN-GWO model. The proposed algorithm unlocks scalability and system adaptability to operational variability by adopting numeric imputation and missing-data-tolerant techniques. The proposed algorithm is evaluated on the 68-bus system and the Northeastern United States 25k-bus synthetic test system with credible contingencies using the PowerWorld simulator. The obtained results prove the enhanced performance of the proposed technique over competitive state-of-the-art transient stability assessment methods under various contingencies with an overall accuracy of 99% within 0.64 s after the fault clearance.

INDEX TERMS Deep learning (DL), grid stability prediction, power system dynamics (PSD), time series data, transient stability.

NOMENCLATURE

$\mathbf{X}_{\text{in}}$	Input embeddings.
Variables	
$\delta_{\max}$	Maximal phase angle discrepancy.
η	Transient stability index (TSI).
$\mathcal{N}_i$	Set of buses adjacent to bus i.
B_{ij}	Imaginary component of the admittance matrix.
G_{ij}	Real component of the admittance matrix.
P^i_{inj}	Real power injection at bus i.
Q^i_{inj}	Reactive power injection at bus i.
t	Time variable spanning the interval $[t_0, T]$.
x	State variables of the system in $\mathbb{R}^n$.

Abbreviations

ACC	Accuracy.
AWGN	Additive white Gaussian noise.
BGRU	Bidirectional gated recurrent unit.
BLSTM	Bidirectional long short-term memory.
CNN	Convolutional neural network.
DBN	Deep belief network.
DKDE	Diffusion-type kernel density estimator.
DL	Deep learning.
DT	Decision tree.

ELU	Exponential linear unit.
F1	F1-score.
FN	False negative.
FP	False positive.
GCNN	Classical convolutional neural network.
GINN	Inception neural network.
GM	Geometric mean.
GPU	Graphical processing unit.
GRU	Gated recurrent unit.
GWO	Grey wolf optimizer.
LSTM	Long short-term memory.
MLP	Multilayer perceptron.
PCC	Pearson correlation coefficient.
PFC	Postfault cycle.
PMU	Phasor measurement unit.
Prec	Precision.
PSD	Power system dynamics.
PWS	PowerWorld simulator.
R	Recall.
RAM	Random access memory.
ReLU	Rectified linear unit.
RES	Renewable energy sources.
RNN	Recurrent neural network.
SCADA	Supervisory control and data acquisition.
SD	Standard deviation.
SNR	Signal-to-noise ratio.
SSD	Solid-state drive.
t-SNE	t-distributed stochastic neighbor embedding.
TCN	Temporal convolutional networks.
TN	True negative.
TNR	True negative rate.
TP	True positive.
TPR	True positive rate.
TrT	Training time.
TSA	Transient stability assessment.
TT	Testing time.
Uns.	Unstable.
WGN	White Gaussian noise.
XGB	Extreme boosting trees.

I. INTRODUCTION

A. MOTIVATION

With the constantly expanding scale of modern power systems, the existing power infrastructure encounters unprecedented changes in the wake of extensive penetration of renewable energy sources (RESs) [1]. However, the power generation from RES is subjected to large disturbances by the natural environment leading to randomness, intermittence, and weak controllability of energy generation [2]. The drastic change in power system dynamics (PSD) due to RES integration jeopardizes system stability [3]. Therefore, the power system stabilizers and turbine governors are pushed to their operational limits [4]. Furthermore, the incorporation of power electronic devices, which possess low or zero inertia, diminishes the system's disturbance tolerance [5]. When the power systems encounter various disturbances, grid stability becomes an inevitable problem for power grid control. Nevertheless, the supervisory control and data acquisition system shows a reduced efficacy for the adoption of wide-area monitoring systems and fast-acting inverter-based resources due to the slow sampling rate [6]. Thus, efficient real-time transient stability monitoring is pivotal for active power balance.

The transient rotor angle stability evaluates a power system's ability to return to normal operation or reach a new state after a severe malfunction [1]. Transient instability can quickly lead to system collapse in just a few seconds following an incident [7]. This can occur when generators experience a decrease or increase in output power, causing rotor acceleration or deceleration [8]. To prevent the collapse of the power grid, transient stability assessment (TSA) attained a surge of interest in power instability prevention in its early stages. This assessment method gives control actions enough time to be executed before the system's collapse [3]. Control actions are typically ascertained by iterating over multiple postcontingency scenarios within the transient window of 0–10 s [9]. Generator rescheduling and load shedding are perceived as effective control measures for enhancing transient stability performance [10]. Yet, the escalating scale and intricacy of contemporary power systems introduce additional challenges to prevent transient instability in different operating environments [11].

B. RELATED WORKS

Extensive literature is dedicated to investigating TSA-based machine learning as a promising solution for addressing sudden contingencies and blackouts. For instance, Zhou et al. [12] employed a gated graph neural network for TSA. The core idea is to produce unstable samples by a conditional generative adversarial network from the New England 39-bus system simulations. Therefore, the proposed model represents a topology change-tolerant and class imbalance resilient by generating its costume data for training. However, the goodness of the generated samples is missed in the conception of the proposed paradigm. Thus, the proposed method is susceptible to falling into erroneous predictions. Yadav et al. [13] implemented a diffusion-type kernel density estimator (DKDE)-based multilayer perceptron for accurate real-time classification of events in power systems. The DKDE is employed to identify the shape of 3-D voltage and frequency distributions over time. With varying levels of renewable penetration, the proposed technique features fast processing with limited computational requirements and high model explainability. Nevertheless, the adopted feature extraction does not consider the various faulty issues in the sensors, thereby limiting the feasibility of the proposed DKDE in practical implementations.

A multitude of specialized deep learning (DL) techniques have been employed for TSA, including deep belief networks (DBNs), recurrent neural networks (RNNs), and convolutional neural networks (CNNs). DBN-based methodologies, as illustrated in [19], incorporate a local linear interpreter to constrain the DBN, albeit without providing a

TABLE 1 Related Research Works of Representation Learning Methods for TSA

Ref.	Pipeline	ACC (%)	Advantages	Drawbacks
[14]	Cascaded Convolutional Neural Networks	99.82	-Adaptability to varying conditions and system topologies; -Continuous refreshing of the early termination criterion via feedback learning.	-Complex model design; -Overfitting risks to training data.
[15]	Stacked Gated Recurrent Unit	100	-Allows parameter sharing in GRU layers; -Has fewer parameters than traditional methods.	-Unbalanced data can affect learning; -Relies heavily on data quality.
[16]	Convolution Algorithm & Deep Forest	98.76	-Manages redundant features well using parallel convolution algorithms and pooling functions; -Strong robustness to hyperparameter variations and class imbalance.	-Requires extensive training; -Can be resource and time-intensive.
[17]	SYNDAE[1]	98.78	-Enhances recognition of unstable samples and reduces misclassification risks.	-Limited model interpretability; -Depends on high-quality data and high computational demand.
[18]	Adaptive Denoising Combined Model	97.34	-Effective in handling data with noise interference; -Can adaptively distinguish the distribution of actual noise.	-Performance can suffer from noise type mismatches; -Potential overfitting to specific noises.

[1] Adaptive SYNthetic sampling based Denoising Auto-Encoder

comprehensive explanation of the entire TSA model. CNNs, renowned for their superior feature extraction capabilities, significantly expedite the training process and enhance the accuracy of the final results. For instance, Zhou et al. [20] developed a CNN-based ensemble method that can be promptly updated with informative samples before substantial alterations occur in the power system. Similarly, the work in [21] employs a twin convolutional support vector machine (SVM) network to predict transient stability by effectively mining the internal structure of trajectory features. In addition, Arteaga et al. [22] demonstrated how power system snapshots can be represented as images, allowing CNNs to directly predict stability status. Yan et al. [23] proposed a technique that combines cascaded CNNs with time-domain simulation, thereby improving computational efficiency for prefault stability assessment by extracting features from various time intervals. Furthermore, the work in [23] introduced a hierarchical and self-adaptive CNN approach to ascertain postdisturbance stability via an integrated decision-making framework utilizing multiple CNNs. On the other hand, Zhang et al. [24] proposed an active transfer learning with DBN for online TSA. DBN model is an efficient DL algorithm for judiciously reducing the dimensionality of features, which makes the system perfectly tailored for TSA using synthetic sets [25]. Unfortunately, the proposed single-event identification restricts its practical usage in various industrial scenarios.

RNNs, including long short-term memory (LSTM) and gated recurrent units (GRU), are adept at processing variable-length input sequences by considering both temporal and spatial correlations. The work in [26] proposed a self-adaptive LSTM model for online TSA, capable of capturing temporal and spatial data dependencies. While Yu et al. [27] introduced an LSTM-based approach for classifying transient stability using multiple time-step algebraic variables. GRU-based methodologies, as detailed in [28] and [29], facilitate real-time transient instability prediction without necessitating fault information, exhibiting robustness against measurement topology changes and noise. Table 1 summarizes some of the emerging TSA-based methods from the literature [14], [15], [16], [17], [18]. While higher model complexity can lead to improved accuracy, as seen in the high scores reported, it often comes at the cost of increased computational demand and potential overfitting. The challenge lies in balancing complexity with practical deployability, especially in real-time systems where quick decisions are crucial.

C. CONTRIBUTIONS

This article presents an efficient TSA method based on temporal convolutional networks (TCNs) and grey wolf optimizer (GWO) to address the TSA challenges posed by the increased complexity of modern interconnected power grids. Herein, the TSA is mapped as a two-class classification problem. The main contributions are summarized as follows.

1) A DL-based approach with efficient feature extraction ability is proposed for TSA status prediction of the power system. The proposed approach provides a lower memory footprint while extracting deep features and long-term temporal relationships through the adoption of TCN and GWO models, where the proposed GWO is employed for TCN hyperparameters' optimization.
2) Unlike existing algorithms, the performance of the proposed TCN-GWO method is validated on a large synthetic power system with high penetration of different types of RES and proved to be of high accuracy.
3) Various data conditions are simulated and findings verify the proposed model's ability to maintain high accuracy and reliability under imperfect data conditions. The conditions considered includes noisy data with different signal-to-noise ratios (SNRs) and scenarios simulating missing and faulty PMU data.
4) The proposed TCN-GWO-based TSA approach is validated through real-time simulation via its implementation on Raspberry Pi 3, where the sensor data are transmitted to the software platform through the network-connected Raspberry Pi. Conversely, the software platform dispatches control signals to thee

Raspberry Pi via the network, thereby facilitating user feedback within the physical environment.

The rest of this article is organized as follows. Section II explores the problem formulation. The transient stability index (TSI) and feature selection are introduced in Section III. The overall framework of the proposed algorithm in the study is outlined in Section IV. Section V presents the simulation results to demonstrate the validity of the proposed DL model. Finally, Section VI concludes this article.

II. PROBLEM FORMULATION

The PSD comprising N buses linked by transmission lines is predominantly influenced by the synchronous generators and their accompanying control strategies [30]. The PSD are governed as

$$\dot{x} = f(x, u) \tag{1}$$

where x encapsulates the dynamic states of various bus dynamics, and u defines the external inputs to the system. The real power (P_{inj}) and reactive power (Q_{inj}) injections at bus i are, respectively, expressed as [31]

$$P^i_{\text{inj}} = G_{ii}V_i^2 + \sum_{j\in\mathcal{N}_i} V_iV_j(B_{ij}\sin(\theta_{ij}) + G_{ij}\cos(\theta_{ij})) \tag{2}$$

$$Q^i_{\text{inj}} = -B_{ii}V_i^2 - \sum_{j\in\mathcal{N}_i} V_iV_j(B_{ij}\cos(\theta_{ij}) - G_{ij}\sin(\theta_{ij})) \tag{3}$$

where θ_{ij} and V_i are the nodal voltage angle and magnitude, respectively. $\mathcal{N}_i$ denotes the set of buses adjacent to bus i, while G_{ij} and B_{ij} represent the real and imaginary components of the admittance matrix, respectively. The above equations are reformulated by differential and algebraic equations to represent the dynamics of the bus system as [32]

$$\dot{x} = f(x, y, u, \xi) \tag{4}$$

$$0 = g(x, y, \xi) \tag{5}$$

where $f(\cdot)$ encapsulates the system's nonlinear differential equation reflecting the controls and dynamics of synchronous generators and loads, and their initial conditions are denoted by x_0. $g(\cdot)$ represents the network and static components. u denotes the operating parameters of the system including the nodal voltages and phase angles of the system at a time variable t spanning from an interval $[t_0, T]$. ξ encompasses all variable resources, such as flexible loads and intermittent RES. The determination of transient stability is based on the maximal phase angle discrepancy $|\Delta\delta|_{\max}$, which is extracted from the state vector x. The interrelation of x and y is given by the nonlinear differential–algebraic system of equations

$$x(t_0 + \Delta t) = x_0 + \int_{t_0}^{t_0+\Delta t} f(x, y, u, \xi))\, dt \tag{6}$$

$$0 = g(x(t_0 + \Delta t), y(t_0 + \Delta t), \xi(t_0 + \Delta t)). \tag{7}$$

The magnitude of the greatest angle of separation between the rotors of any two generators throughout the simulation period $|\Delta\delta|_{\max}$ is determined as

$$|\Delta\delta|_{\max} = \max\left\{|\delta_i(t) - \delta_j(t)| \quad \forall i, j \in \{1, \ldots, n\}, t \in [t_0, T]\right\}. \tag{8}$$

III. TSI AND FEATURE SELECTION

This section presents an overview of the ground truth TSI and delves into the intricacies of the feature selection process.

A. GROUND TRUTH TSI

The ground truth in this study is obtained based on the TSI denoted by η, where the system stability status depends on the postfault rotor angle dynamics. The TSI is defined as follows [33]:

$$\eta = \frac{180^o - |\Delta\delta|_{\max}}{180^o + |\Delta\delta|_{\max}}. \tag{9}$$

One or more generators lose their synchronization when $|\Delta\delta|_{\max} > 180^\circ$ then $\eta \leq 0$, and the system is defined as transient unstable, otherwise, the system is defined as transient stable. Thus, the ground truth or class, c of time instance i, is decided stable or unstable as follows:

$$c(i) = \begin{cases} \text{Stable}, & \eta > 0 \\ \text{Unstable}, & \eta \leq 0. \end{cases} \tag{10}$$

B. SELECTIVE DIMENSIONALITY REDUCTION

1) HIGH FEATURE–FEATURE CORRELATION ELIMINATION

Power systems are large-scale, complicated physical systems with massive features and measurement data. Large dimensionality increases the model complexity and may confuse the learning process. Thus, this study applies the feature–feature correlation reduction techniques based on the Pearson correlation coefficient (PCC). The linear correlation is calculated between every two features and a correlation threshold is set to 0.9. When the correlation coefficient between two features is greater than the threshold, the first feature will be removed from the feature set. The correlation coefficient is calculated as follows [34]:

$$\text{PCC}_{x,y} = \frac{\sum_{i=t}^{T}[(x_i - \bar{x})(y_i - \bar{y})]}{\sqrt{\sum_{i=t}^{T}(x_i - \bar{x})^2 \sum_{i=t}^{T}(y_i - \bar{y})^2}} \tag{11}$$

where $\text{PCC}_{x,y}$ is the correlation coefficient between feature x and feature y, which has a mean of $\bar{x}$ and $\bar{y}$, respectively. Considering the dynamics of the power system in the postdisturbance period, $i = t$ and T are the starting time instant and the simulation time, respectively. Although this approach reduces dimensionality and feature–feature high correlation, it may drop the relevant feature to the target class identification. Thus, this study applies a feature ranking technique before highly correlated feature elimination.

2) FEATURE RANKING STAGE

Feature ranking and feature selection help identify the relevant features to the target. By adopting the adequate feature subset selection algorithm, the system's exploitability in real-time

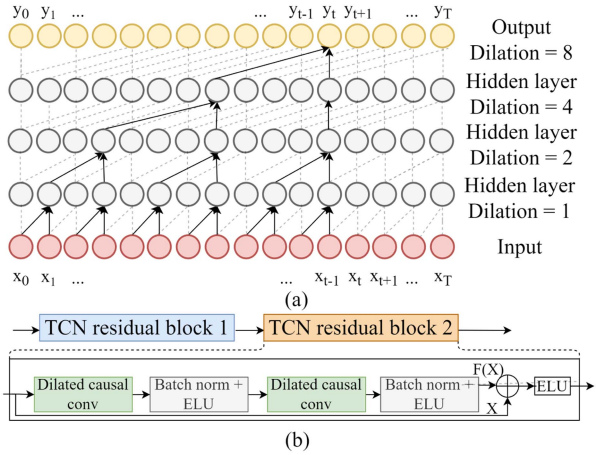

FIGURE 1. Flowchart of (a) conceptual diagram of a stack of dilated causal convolutions and (b) architecture of the TCN consisting of two residual blocks.

implementation is significantly promoted by its minimalistic set of features, which not only adds to its simplicity but also enhances its interpretability and reduces its computational requirements [35]. This article employs extreme boosting trees for feature ranking [36]. The approach maximizes a feature set's relevance to the answer variable while minimizing its inconsistency [37].

3) FORWARD FEATURE SELECTION

Lastly, forward feature selection is applied to ensure efficient performance, where model training is an iterative process, each iteration adds one more feature to the feature set and records the model performance. Finally, the best-performing feature set is selected.

IV. PROPOSED METHODOLOGY

This section provides a detailed overview of the proposed methodology. We begin by introducing the fundamentals of the TCN model, followed by an explanation of the GWO technique. Lastly, we present a comprehensive discussion of the intelligent classifier employed in our approach.

A. TCN MODEL GENERALITIES

TCN is a monodimensional CNN variant designed to fully understand the hidden temporal dependencies in the abundant time series data [38]. Therefore, the TCN model is perfectly tailored to model the temporal dynamic behavior of power systems. Multiple studies validate the outperformance of TCN over various state-of-the-art models, such as CNNs and LSTMs. The TCN is able to identify temporal correlations in the features due to its integration of CNN's feature extraction capabilities and RNN's ability to model time-series data. TCN consists of a stack of residual blocks hierarchically distributed, as shown in Fig. 1(a). The TCN architecture contains dilated-causal convolution followed by batch normalization and ELU activation, as shown in Fig. 1(b). Xia et al. [39]

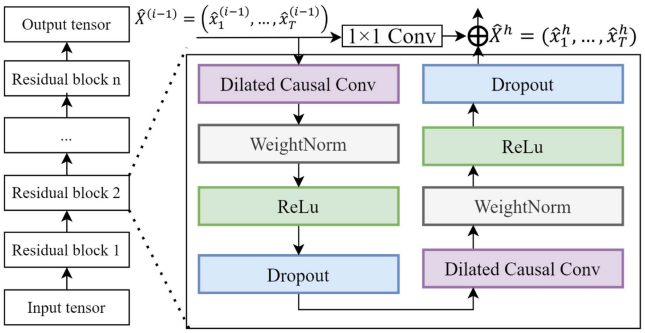

FIGURE 2. Architecture of TCN with *n* residual blocks.

improved the basic structure of TCN by incorporating residual connectivity and regularization. The original 1-D causal convolutional layer is replaced by a residual block with two layers having the same expansion privacy and residual connectivity, as shown in Fig. 2. The receptive field size r can be obtained by [39]

$$r = 1 + \sum_{i=0}^{n-1} 2(k-1)b^i = 1 + 2(k-1)\frac{b^n - 1}{b-1}. \tag{12}$$

The convolution kernel size is denoted by k, while the dilation base is denoted by b, and it must satisfy the condition $k \geq b$. The number of residual blocks (n) is determined based on the length of the input tensor and can be calculated as described in [39]

$$n = \left\lceil \log_b \left(\frac{(l-1)(b-1)}{2(k-1)} + 1 \right) \right\rceil. \tag{13}$$

To ensure that the residual block maintains the same length between input and output, a 1-D fully convolutional network architecture is utilized. The use of dilated causal convolution W ensures that the output remains unaffected by future information. The dilated convolution is computed as [40]

$$W(s) = (x * df)(s) = \sum_{i=0}^{k-1} f(i) \times X_{s-d.i} \tag{14}$$

where $f : 0, \ldots, k-1$ represents the convolution filter, while k denotes the kernel size. The dilation factor, d, signifies the gap between convolution kernels, and $s - d.i$ corresponds to the convolution involving only the previous time state. The residual connection can be represented as [41]

$$o = \text{Activation}(x + F(x)). \tag{15}$$

The activation function, which may include rectified linear unit (ReLU) and Sigmoid, is used in the TCN architecture. During the offline training phase, the TCN is trained using simulation data. In the online assessment phase, the TCN assessment model is triggered whenever a fault is detected. If the system is deemed unstable, the TCN will provide additional information to support the implementation of emergency control strategies.

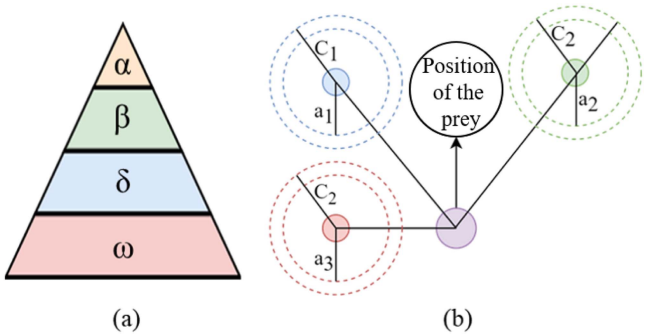

FIGURE 3. Mechanism of the (a) ranking of grey wolf pack and (b) position adjustment for the GWO technique.

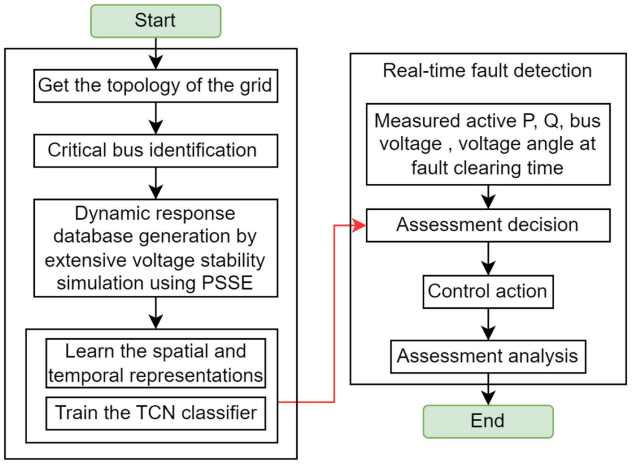

FIGURE 4. Process of the proposed TCN-based transient stability predictor.

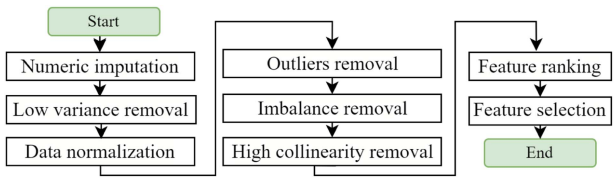

FIGURE 5. Flowchart of data processing steps.

B. GREY WOLF OPTIMIZER

The GWO is a bio-inspired, swarm-centric metaheuristic optimization technique. The GWO draws its inspiration from the hunting patterns and pack hierarchy observed in grey wolves. This algorithmic approach mirrors the social dynamics and the predatory tactics of these animals. Within the pack, the beta wolf (β) is considered the second in command, offering counsel and support. The role of the delta wolf (δ) encompasses scouting and providing wisdom, whereas the omega wolves (ω) are typically involved in more subordinate tasks, including looking after young wolves.

The alpha wolf (α) is the pack leader, exerting dominance and making key decisions. The social structure is depicted in Fig. 3(a). In addition, the GWO mimics the wolves' hunting technique, which involves surrounding, pursuing, and ultimately capturing prey, as illustrated in Fig. 3(b). In this model, the position of the wolves is dynamically adjusted during the hunt, informed by the leading wolves (α, β, δ), to effectively encircle the prey. The mathematical formulation for the encirclement strategy is provided in [42]

$$\overrightarrow{D} = \left| \overrightarrow{C} \times \overrightarrow{X_p(t)} - \overrightarrow{X(t)} \right| \tag{16}$$

$$\overrightarrow{X(t+1)} = \overrightarrow{X_p}(t) + \overrightarrow{A} \times \overrightarrow{D} \tag{17}$$

where X_p represents the prey's position, while t refers to the number of iterations. The vector $\overrightarrow{A}$ signifies the coefficient vector. The distances between the prey and other grey wolves are denoted by $\overrightarrow{D_\alpha}$, $\overrightarrow{D_\beta}$, and $\overrightarrow{D_\delta}$, respectively. The computation rules for the vectors $\overrightarrow{A}$ and $\overrightarrow{C}$ are as follows [42]:

$$\overrightarrow{A} = 2\overrightarrow{a} \times \overrightarrow{r}_1 - \overrightarrow{a} \tag{18}$$

$$\overrightarrow{C} = 2 \times \overrightarrow{r_2} \tag{19}$$

where $\overrightarrow{r_1}$ and $\overrightarrow{r_2}$ are random number vectors. The GWO algorithm caught researchers' attention from various engineering areas. However, the application of the GWO to TSA has not been extensively investigated, prompting us to investigate its capability in handling highly nonlinear temporal dependencies in the TSA paradigm. The GWO is selected to identify the best sets of TCN hyperparameters for its excellent optimization accuracy. Furthermore, GWO is evaluated against five other hyperparameter optimization techniques to highlight its outstanding performance. These techniques are simulated annealing (SA), particle swarm optimization (PSO), random search (RS), evolution strategy (ES), and Bayesian optimization (BO) [43].

C. PROPOSED METHOD

The proposed method is shown in Fig. 4. Specifically, the proposed method starts with getting the topology of the grid. Initially, the power grid's topology is acquired. In order to generate useful data, the proposed system targets the critical buses using trial and error to apply the faults. Faults are simulated on critical buses, generating data, such as bus voltages V_i, voltage angles θ_i, frequency F_i, reactive power Q_i, and active power P_i. Next, a dedicated data processing strategy is applied, as shown in Fig. 5.

A concise data processing protocol for TSA begins with numeric imputation to address missing values in data. This step is followed by the elimination of low-variance features, which are statistically unlikely to influence the TCN predictive accuracy due to their minimal variation. The dataset is then normalized, allowing different scale features to contribute equally to the analysis. Subsequently, outlier removal purges anomalous data points that could otherwise distort the model's predictive capabilities. To prepare the data for balanced modeling, imbalance removal is implemented, correcting skewed distributions that could bias the model toward the majority

Algorithm 1: Proposed TCN-GWO Method.

Input: Power grid data stream D, critical buses set B
Acquire topology of the power grid
Identify critical buses $B_c \subset B$
for each critical bus b_i in B_c
  Simulate faults on b_i, generating data D_i
  Process data D_i with numeric imputation and normalization
  Remove low variance and outliers from D_i
  Balance the dataset D_i to form D_{final_i}
  Reduce collinearity and select relevant features from D_{final_i}
  Optimize TCN hyperparameters θ_{TCN} using GWO
  Train TCN model with D_{final_i} and θ_{TCN}
  Produce TSA result TSA_{result_i}
  Determine control actions based on TSA_{result_i}
end for
Output: Control actions to prevent instability

class. High collinearity features are also discarded to prevent overfitting and ensure that the model relies on independent predictors. With the data refined, feature ranking assesses the relative importance of each variable, leading to a judicious feature selection leading to a refined dataset D_{final}. The GWO optimizes the hyperparameters θ_{TCN} for the TCN model. The TCN model, trained on D_{final} and θ_{TCN}, outputs a TSA result $\text{TSA}_{\text{result}}$. Based on this result, appropriate control actions are determined, ensuring efficient and effective decision-making in the power system's operation. To prevent system instability, these control actions can range from adjusting generator outputs to implementing load shedding and system reconfiguration. The proposed algorithm is further described in Algorithm 1.

V. SIMULATION RESULTS

This section demonstrates the feasibility and effectiveness of the proposed method using multiple simulations. Two bus systems of different scales are discussed: the IEEE 68-bus system and the ACTIVSg25k-bus power system.

A. SIMULATION SETUP

A systematic simulation setup is employed to develop a comprehensive dataset for TSA. The IEEE systems are subjected to disturbances to generate transient stability with stable and unstable samples for training and testing. In the final training dataset, the stable/unstable ratio is approximately 1:1. The system stability is judged at the end of the simulation. The subjected disturbance considered is the three-phase short-circuit grounding faults since they portray the most severe disturbance in a network compared to other types of faults, at selected critical buses. The subjected faults are precisely located at the bus terminals and subsequently cleared. To introduce variability and enhance the robustness and diversity of the dataset, the fault clearance times are randomly selected to fall within a range of 0.1–10 s. That is coinciding with the span of the simulation time with a sampling frequency of 100 Hz (0.01 s).

Fig. 6 depicts the generator rotor angles under different severity scenarios following short-circuit faults at critical buses: where Fig. 6(a) and (b) represents less severe and more critically severe conditions, respectively, while Fig. 6(c) captures an unstable scenario. Data acquisition concludes the simulation, and once the fault is cleared, critical parameters include the active (P) and reactive (Q) power for all lines, alongside voltage magnitude (V), frequency (F), and phase angle (θ) for each bus, are captured to form the feature space, as shown in Fig. 7. This TSA system plays a significant role in predicting stability issues in real time, enabling proactive adjustments and interventions in the grid's operation. These data form the basis for assessing system stability, and each time sample is classified based on (10).

The samples are generated for each bus system, to balance the number of stable and unstable samples. The acquired data are simulated through detailed time-domain simulations using the commercial software PowerWorld Simulator (PWS) version 23. The numerical simulations are performed using Python 3.8 on a Lenovo IdeaPad L340 running on an environment powered by a NVIDIA GeForce GTX 1650 4 GB dedicated graphics and a 9th Generation Intel Hexa-Core i7-9750H Processor, six cores, 12 M Cache CPU @ 2.60 GHz with an installed memory (RAM) of 16 GB, and 256 GB solid-state drive. All data analytics experiments have been implemented via Google Colab Pro Plus with High-RAM, A100 graphical processing units (GPU), and background execution options enabled. The used platform features preinstalled packages, which reduces potential errors due to the compatibility of all the versions. All comparison results are based on ten repeated simulation trials for each IEEE bus system to obtain a mean value of recognition metrics.

To further investigate the TCN performance, the t-distributed stochastic neighbor embedding (t-SNE) is used to visualize and map the high-dimensional space into a 2-D space. Fig. 8 shows that the stable and unstable samples are interspersed in the original feature space. However, the separation into two distinct clusters differs from one bus system to another, which stresses the learning algorithm. As observed in Fig. 8(a), there are many overlapping regions in the feature space. Thus, the separability of samples is poor. This makes it intuitively difficult to identify unstable cases in the representation space as compared to the original feature space. In Fig. 8(b), most of the samples have a diverse distribution and are far away from the class decision boundaries of the stable and unstable samples.

This demonstrates that training models in environments with frequent topological changes are particularly challenging due to the risk of overfitting. GWO is proposed as an effective optimization strategy that is essential to address this issue. Table 2 comprehensively compares different hyperparameter optimization techniques applied to a proposed model on the

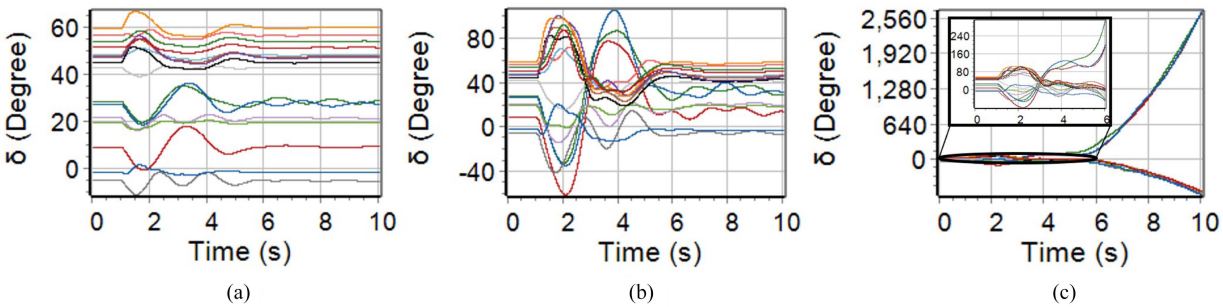

FIGURE 6. (a) Transient stable case with a less severe fault, (b) transient stable case with a very severe fault, and (c) transient unstable case.

TABLE 2 Comparison of Hyperparameter Optimization Techniques on the IEEE 68-Bus System

Configuration	Search Space	Optimization Methods					
		GWO	SA	PSO	RS	ES	BO
Number of layers	[2,5]	3	2	2	2	2	2
Kernel size	[1,5]	3	5	5	5	1	1
Number of filters	[8,64]	52	64	64	64	64	64
Activation	[Sigmoid, Tanh, ReLU]	ReLU	ReLU	Sigmoid	Sigmoid	Sigmoid	ReLU
Learning rate	[0.001,0.1]	0.004	0.1	0.001	0.1	0.001	0.1
Accuracy		99.11	97.33	97.86	97.6	98.31	98.22
Total Time (s)		1859.33	1436.15	2369.63	2794.57	1843.7	1045.8
Time/iteration (min)		3.09	2.39	3.95	4.66	3.07	1.74

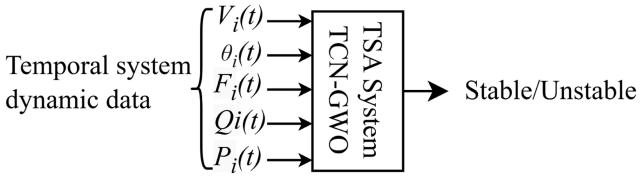

FIGURE 7. Feature inputs of the TSA system.

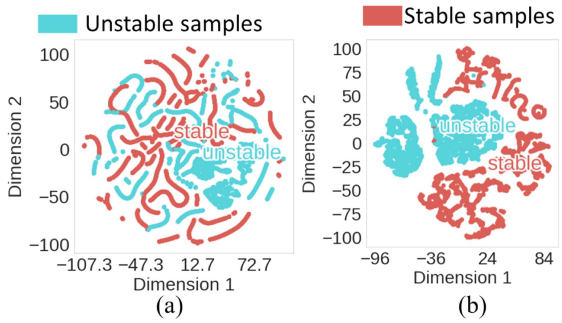

FIGURE 8. 2-D visualization of sampling strategy behaviors with t-SNE. (a) 68-bus system. (b) ACTIVSg25k-bus system.

IEEE 68-bus system. It succinctly outlines the various configurations tested and the outcomes achieved through different optimization methods, including key model parameters, such as the number of layers, kernel size, number of filters, activation function, and learning rate. To ensure a fair comparison, each optimizer completed 30 iterations. From Table 2, it can be seen that there are three TCN layers, each having a dropout rate of 0.5. The chosen activation function is ReLU. The learning rate is 0.004 with a kernel size of 3 and 52 filters. These identified hyperparameters are applied to tune the model, regardless of changes in the bus system. Performance metrics, such as accuracy, total computation time, and time per iteration, are listed for each method. GWO notably achieved the highest accuracy at 99.11%, suggesting its superiority in optimally adapting the model parameters for this specific task. On the other hand, BO excelled in efficiency, with the lowest total time and time per iteration among all methods. It is worth mentioning that the hyperparameter optimization methods other than GWO failed to optimize the model designed for the ACTIVSg25 k bus system.

B. EVALUATION MEASURES

In this study, the proposed method's effectiveness is evaluated using the accuracy (ACC), precision (Prec), recall (R), F1-score (F1), and geometric-mean (GM). The mathematical formulas for these measures are also provided [44]

$$\mathrm{ACC} = \frac{T_P + T_N}{T_P + T_N + F_P + F_N} \tag{20}$$

$$\mathrm{Prec} = \frac{T_P}{T_P + F_P}, \quad R = \frac{T_P}{T_P + F_N} \tag{21}$$

$$F1 = 2 \times \frac{\mathrm{Prec} \times R}{\mathrm{Prec} + R}, \quad \mathrm{GM} = \sqrt{\mathrm{TNR} \times \mathrm{TPR}} \tag{22}$$

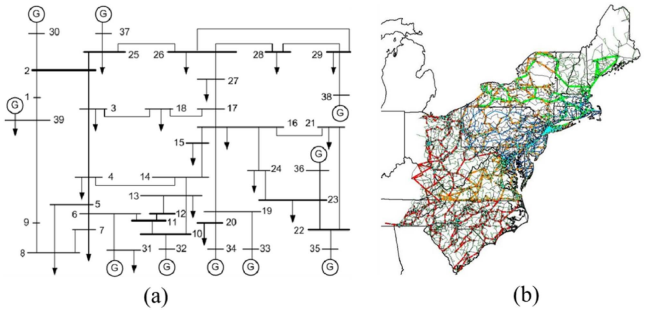

FIGURE 9. One-line diagram for (a) the IEEE 68-bus system and (b) the synthetic 25k-bus Northeastern United States system [46].

TABLE 3 Description of the Knowledge Base

System	68-bus system			ACTIVSg25k-bus system		
Set	Total	Stable	Uns.	Total	Stable	Uns.
Total	68 800	34 411	34 389	24 004	12 021	11 983
Train	48 160	24 088	24 072	16 803	8415	8388
Test	20 640	10 323	10 317	7201	3606	3595

where T_P, T_N, F_N, and F_P denote true positive, true negative, false negative, and false positive, respectively. TPR and TNR are the true positives rates and true negatives rates, respectively. Moreover, the computational time is assessed. Here, the training time (TrT) reveals the GPU time of the training process, and the testing time (TT) denotes the time required for the online application process.

C. IEEE 68-BUS SYSTEM: FEASIBILITY STUDY

To further validate the performance of the proposed risk assessment method, the 16-machine 68-bus test system is used [45]. This system has 16 machines, 86 transmission lines, and five areas, representing a reduced version of the New England test system linked with the New York power system, as shown in Fig. 9(a) [45]. The IEEE 68-bus system provided a total of 68 800 samples, split nearly evenly between 34 389 unstable and 34 411 stable contingencies, as given in Table 3. These samples were distributed across three distinct sets: training and validation (70%), and testing (30%). Specifically, the IEEE 68-bus system's training and test sets comprised 48 160 and 20 640 samples, respectively. To analyze the proposed method convergence, performance curves depicting the results are shown in Fig. 10. According to Fig. 10, the results show that the proposed model reaches the state of convergence after 30 epochs. The model has a fast convergence in terms of the loss function from the fourth epoch. To obtain a more objective model accuracy, Table 4 presents the tenfold cross-validation results of the TCN-GWO method. SD stands for the standard derivation. According to Table 4, the proposed method is found highly performing with an overall accuracy of 98.54% and precision of 98.56%. It is worth mentioning that the model performance has a minor standard deviation of 0.38%, which proves the robustness of

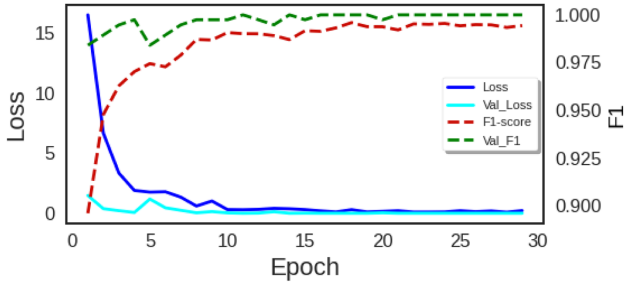

FIGURE 10. Diagnostic evaluation indicators F-1 and loss.

TABLE 4 TCN Performance Measures for Tenfold Cross-Validation, test on IEEE 68-Bus System

Fold	ACC (%)	Prec (%)	R (%)	F1 (%)	GM (%)
1	98.22	98.23	98.22	98.22	98.22
2	97.96	97.96	97.97	97.96	97.96
3	98.40	98.43	98.42	98.40	98.40
4	98.31	98.35	98.33	98.31	98.31
5	98.49	98.50	98.50	98.49	98.49
6	98.40	98.43	98.42	98.40	98.40
7	98.49	98.52	98.51	98.49	98.49
8	99.02	99.02	99.03	99.02	99.02
9	99.11	99.11	99.12	99.11	99.11
10	99.02	99.04	99.02	99.02	99.02
Mean	98.54	98.56	98.55	98.54	98.55
SD	0.38	0.38	0.38	0.38	0.38

TABLE 5 Comparative Results on the IEEE 68-Bus System

Model	TCN-GWO	GCNN [48]	GINN [48]	DT [49]
ACC (%)	98.54	97.22	98.40	95.01

the TCN method in providing a reliable prediction based on fair assessment from tenfold cross-validation. The reported results demonstrate the high performance of the proposed model for the TSA application.

To benchmark the proposed TCN-GWO model, systematic comparisons are made with the approaches presented in [47] and [48]. The compared models include the classical convolutional neural network (GCNN) [47], inception neural network (GINN) [47], and the decision tree (DT) classifier [48] for TSA on the IEEE 68-bus system. GCNN employs two convolutional layers for quick execution compatible with data sampling rates, whereas GINN utilizes inception blocks in its advanced CNN architecture for enriched feature extraction without a significant increase in computational demand. The DT classifier uses postfault cycles (PFCs) of voltage samples for input. Table 5 showcases the accuracy comparison of the proposed model with other state-of-the-art models in the IEEE 68-bus system.

Table 5 demonstrates the superior accuracy of the proposed TCN-GWO method over the methods presented in [47] and [48]. According to Table 5, the GCNN and GINN models

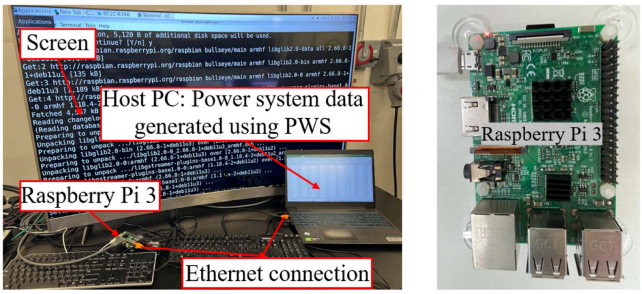

FIGURE 11. Time domain simulation of TCN method using a Raspberry Pi 3. (a) Experimental setup. (b) Raspberry Pi 3.

scored 97.22% and 98.4%, respectively [47]. The DT classifier predicts over 95% of unstable contingencies without any PFC data and achieves a mean accuracy exceeding 97% with 60 PFCs [48]. The proposed TCN-GWO method outperforms the other approaches with an accuracy of 98.54%.

The proposed system deploys a TCN-GWO on a Raspberry Pi 3, equipped with a Quad Core 1.2 GHz Broadcom BCM2837 64 b CPU with 1 GB on-chip RAM and 32 GB Micro SD, optimized for real-time TSA in power systems. To ensure the adequacy and capacity of the deployed solution, a TCN-GWO model is converted through TensorFlow lite, handling real-time data processing on the device. The experimental setup is seen in Fig. 11. According to Fig. 11, the data information collected by the sensors are sent to the terminal application through the Raspberry Pi connected to the network, and the software platform sends control signals to the Raspberry Pi through the network to realize feedback to the user in physical space. In this study, measurement data are processed locally using a USB device to minimize latency, with the option to relay data to a Google Drive platform for extended analysis. A Python 3.9 environment is used, displaying real-time and historical data through graphs and charts. The system is connected to the Internet while real-time domain simulations validate the model's performance under various grid conditions. Fig. 12 illustrates a block diagram for TSA in power systems leveraging a TCN-GWO algorithm and implemented on a Raspberry Pi 3. The process initiates with the assessment start, where PMU measurements are taken immediately after a fault occurrence. These measurements are processed by a trained TCN-GWO model deployed on the Raspberry Pi. The model assesses the current state of the system and decides whether it is stable. If the system is deemed unstable, a control action is triggered to rectify or mitigate the instability. Following the control action, an assessment analysis is conducted to evaluate the effectiveness of the intervention, after which the assessment process concludes. This flow emphasizes real-time monitoring and rapid response to ensure the system's stability. The proposed model has been developed and tested to ensure high efficiency and accuracy in scenarios where real-time data processing is critical. Table 6 presents the simulation results of the proposed

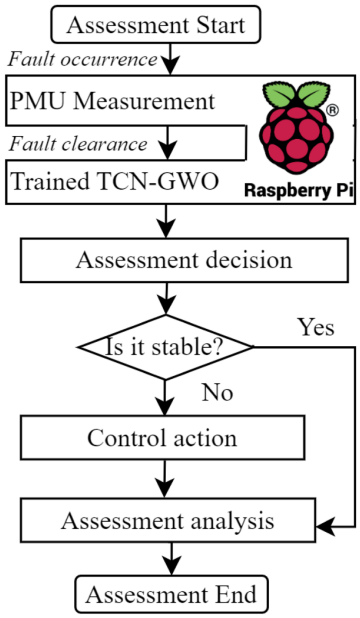

FIGURE 12. Block diagram of the TCN-based TSA with Raspberry Pi 3.

TABLE 6 Performance Metrics of the TCN-GWO Model Implemented on Raspberry Pi 3

Model	ACC (%)	Prec (%)	F1 (%)	Test time (ms)
Prop.	98.98 ± 0.4	98.97 ± 0.4	98.98 ± 0.4	0.672 ± 0.001

model. According to Table 6, the obtained results presented demonstrates the model's exceptional performance across several metrics. The ACC, Prec, and F1 score are all remarkably high, nearly reaching perfection at approximately 98.98%. In addition, the model demonstrates outstanding efficiency with an average test time of only 0.672 ms per instance. This rapid processing capability makes the TCN-GWO model highly suitable for real-time dynamic system monitoring in TSA.

D. MODEL SENSITIVITY TO DATA QUALITY

To evaluate the proposed model's robustness against different data quality levels, the following three tests were performed:

1) involving data with varying levels of noise across different training ratios;
2) fixed training ratio across different noise levels;
3) involving missing data.

Fig. 13 summarizes the obtained results against different data qualities.

For the first test, white Gaussian noise (WGN) is added to the data at varying percentages with an SNR of 34 dB, which is approximately 2%, followed by repeating the training process with diverse training ratio percentages [48]. To model the impact of WGN on the signal, let s represent the pristine signal and n the additive WGN. The perturbed signal x is then expressed as $x = s + n$, where n is the Gaussian distribution with a zero mean and a variance of σ^2, symbolized as $\mathcal{N}(0, \sigma^2)$ [49]. Fig. 13(a) presents a comparative analysis

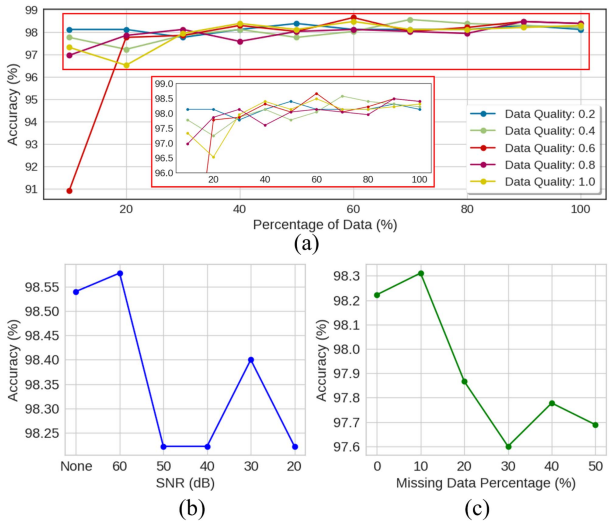

FIGURE 13. Performance of the TCN-GWO on IEEE 68-bus system against varying data qualities: (a) involving noisy data with various training ratios, (b) fixed training ratio across different noise levels, and (c) involving missing data.

of model accuracy against the size of training data and data quality levels.

Regarding Fig. 13(a), the model shows a significant resilience to decreasing data quality levels, with a maximum accuracy drop of 0.62%. Even with 60% data quality reduction, performance only suffers a marginal reduction. The graph shows that even with lower data quality, accuracy can be significantly improved with the increase in data percentage used for training. However, at a data quality level of 0.2, there is a stark variability in performance, suggesting that poor data quality can lead to less reliable model outcomes. Furthermore, the most substantial noise levels introduced in this experiment exceed the noise thresholds set by the IEEE C37.118.1-2011 standard by nearly double, illustrating the model's ability to maintain high accuracy in real-world scenarios compared to this test's severe conditions [50].

The second test includes varying the SNR value and applying noise to all measurements introducing noise to the PMU data to simulate a noisy measurement scenario. The noise in PMU data has a standard deviation ranging from 0.0005 to 0.01, resulting in a typical SNR of 45 dB. Fig. 13(b) exhibits the performance of TCN for TSA predictions under a certain value of noise. According to Fig. 13(b), when SNR reduces to 40 dB (higher than the typical SNR), the performance still maintains at a high level, i.e., only a 0.32% decrease in accuracy. The model maintains stable performance for strong noise levels with an SNR of 20 dB. Hence, the proposed model is robust against the noise in PMU data. Furthermore, random values were set to zero in examining the model's robustness to PMU data inconsistencies to emulate the effect of missing data. The resilience of the model is evident from the analysis presented in Fig. 13(c); even when up to 50% of the data are missing, the model sustains high accuracy levels, with only a slight decrease of 1.60% from the ideal state.

TABLE 7 Effect of Faulty and Lost PMU Data on the Performance of the TCN-GWO Model

Scenario	ACC (%)	Prec (%)	GM (%)	F1 (%)
One Faulty PMU	99.20	98.37	99.18	99.18
Three Faulty PMUs	99.00	98.36	98.97	98.97
Five Faulty PMUs	98.40	98.74	98.33	98.33
One Missing PMU	99.00	97.97	98.98	98.97

In the evaluation of the TCN-GWO performance, various scenarios were considered to assess the resilience of the monitoring system. When one PMU is faulty, and provides incorrect readings or the PMU data are lost, there is a notable impact on the performance metrics. Therefore, the following four different scenarios are considered in this study:

1) one PMU provides incorrect readings;
2) three PMUs are faulty;
3) five PMUs provide incorrect data;
4) the data from one PMU are missing.

Each of these scenarios provided valuable insights into the system's ability to withstand and adapt to imperfect conditions. When a PMU is compromised, it is presumed that all readings taken from that unit are assumed as zero as referred to in [51]. Table 7 provides the optimized TCN-based TSA performance under the aforementioned scenarios.

According to Table 7, the accuracy and F1-score remained high across all scenarios, with a single faulty PMU achieving the best metrics at 99.20% and 99.18%, respectively. Even with three faulty PMUs, accuracy marginally decreased to 99.00%, and the F1-score to 98.97%. Notably, a significant performance dip occurred with five faulty PMUs, dropping to 98.40% accuracy and 98.33% for both the GM and the F1-score. A scenario with one missing PMU resulted in slight reductions in precision and F1-score but maintained 99% accuracy, showing that the system is more affected by faulty data than by the absence of data. These findings indicate that the proposed model can handle both data loss and faulty data with high accuracy.

E. ACTIVSG25K-BUS SYSTEM: SCALABILITY STUDY

To illustrate the issues raised in this study and to evaluate the effectiveness and scalability of the proposed method in a large-scale real-world system with high photovoltaic (PV) penetration, this section presents a 25 000-bus synthetic power grid (ACTIVSg25 k) that is built on the geographic footprint of the northeast and mid-Atlantic Interconnection of the United States, as shown in Fig. 9(b) [46]. The test system is a realistic synthetic system created only on geographic and statistical data for planning and stability studies [52]. The simulated area includes 227 generators of which 116 are modeled as solar, 1109 transmission lines, 385 transformers, and 1148 buses. It is designed to supply a demand of 10 104 MW and 2693 MVar spanning nine voltage levels (345/138/69/24/22/20/18/13.8/1 kV) [53]. The area contains five fuel types including coal, natural gas, nuclear

TABLE 8 Performance Comparison of Different Classifiers, test on ACTIVSg25-k Bus System

Model	ACC (%)	Prec (%)	F1 (%)	TrT (s)	TT (s)
GRU	99.13	99.13	99.13	251.39	3.69
LSTM	96.00	96.06	95.99	86.03	3.56
RNN	46.20	23.78	31.60	30.82	1.11
BGRU	98.20	98.23	98.20	169.30	6.51
BLSTM	98.87	98.87	98.87	196.58	5.66
TCN-GWO	99.37	99.38	99.38	175.74	0.64

power, hydropower, and solar, where the solar penetration is approximately 10%. Generators are designed with their appropriate machine and control models to capture their effect on the system dynamics. The IEEE 25k-bus system yielded 24 004 samples, with 12 021 unstable and 11 983 stable contingencies, as given in Table 3. These samples were distributed across two distinct sets: training (70%) and testing (30%). For the IEEE 25k-bus system, the corresponding sets included 8415 and 3606 stable contingencies, and 8388 and 3595 unstable contingencies, respectively.

To model the solar and wind generator models, various combinations of models are used in PWS. The solar dynamics model consists of the machine model REGC_A and the exciter model REEC_A. The machine model represents the utility interface and the electrical control module is the exciter model. The wind generator model consists of the machine model WT3G1, exciter WT3E1, governor WT3T1, and stabilizer WT3P1. Here, the machine model denotes the power electronic converter, the exciter represents the electrical controller, the governor symbolizes the mechanical drive train, and the stabilizer serves as the blade pitch controller.

Based on the previously defined performance indices, the performance of the developed TCN predictor is thoroughly evaluated and compared with other classifiers. Table 8 presents the performance metrics of multiple DL models. These models include GRU, LSTM, RNN, bidirectional gated recurrent unit (BGRU), and bidirectional long short-term memory (BLSTM). All studies are performed on the same training and testing dataset as well as having the same hyperparameters. As seen in Table 8, the original RNN provides an accuracy of 46.20%, which reflects the poorest ability to accurately predict the transient status of the system. On the other hand, the LSTM and BLSTM models exhibited an enhanced performance with 96% accuracy. The GRU and BGRU models provide an accuracy of 99.13% and 98.20%, respectively. This indicates that the proposed TCN classifier can effectively identify stable and unstable patterns in the dataset and maintain a high accuracy of 99.37%. According to Table 8, the proposed model is performing best with precision and F-1 scores of 99.38% and 98.87%, respectively. The achieved accuracy of the TCN model is better than the competitive models. Fig. 14 compares the proposed model performance and verifies its scalability with the change of the IEEE bus systems using the confusion matrix index. According to the confusion matrix from Fig. 14, the proposed system is found

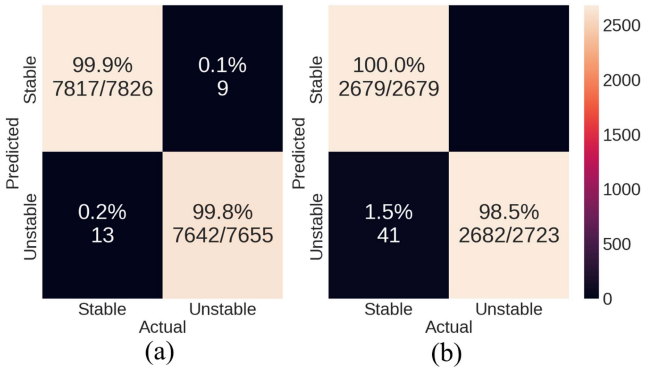

FIGURE 14. Classification performance of the TCN model on (a) IEEE 68-bus system and (b) ACTIVSg25k-bus system based on confusion matrix.

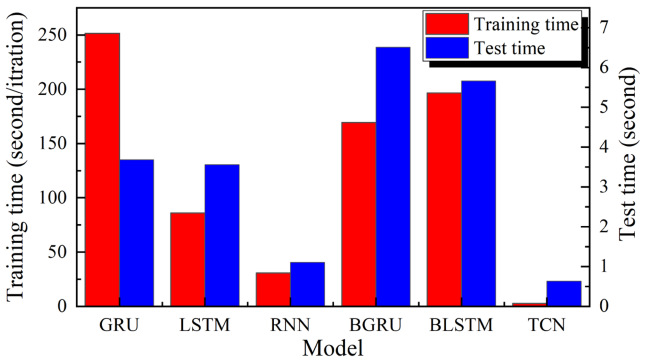

FIGURE 15. Computational time for different evaluation models, tested on the ACTIVSg25-k bus system.

to perform well with all the benchmark datasets from different IEEE bus systems. The minimum performance is found to be 98%. The model's efficiency and flexibility in IEEE bus system applications have been validated. In addition, the necessity for labeled data to achieve satisfactory accuracy does not substantially escalate with the scaling up of the system. Fig. 15 presents the computational time for different evaluation models.

Regarding Fig. 15, the TCN model has a TrT of 175.74 s. Under the same environment, the GRU model requires 251.39 s to complete its training cycles. Moving to the testing phase, the TCN model generates the TSA result in only 0.64 s, which matches the industrial implementation requirements. While the LSTM and BGRU models require 3.56 and 6.51 s to process the final result, respectively. The TCN model assesses the transient stability status less than 640 ms after the short-circuit clearance. This leads to saying that the proposed model is providing the most accurate result in the shortest time, which demonstrates its high applicability in real-world environments. Furthermore, for memory requirements, the proposed model for the 68-bus system is approximately 2.94 MB, and for the 25k-bus system, it is approximately 12.07 MB. The model size increases by 311.37% when the system size expands from 68 buses to 25 k buses, a system size increase of 36 664.71%. The ratio of the model size growth to the power

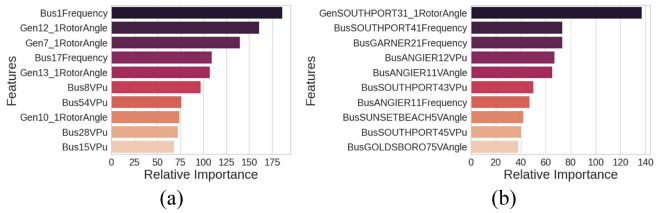

FIGURE 16. Feature importance using LightGBM for (a) 68-bus system and (b) 25 k bus system.

system size growth is approximately 0.85%, indicating that the model scales efficiently in comparison to the significant expansion of the power system, underscoring the potential scalability of the approach for larger and more complex networks.

To gain deeper insights into the factors most influential on prediction results, a feature importance analysis is conducted using the light gradient-boosting machine (LightGBM) algorithm [54], which is widely recognized for feature ranking. This approach clarifies how each feature contributes to the model's decisions. Notably, when a fault occurs, it significantly impacts the measurements of the surrounding buses, underscoring the critical role of fault location. However, the data used in this study encompass various faults across multiple locations. Therefore, conclusions are drawn based on the type of feature rather than its specific location. Fig. 16 presents a summary of the feature ranking analysis for the two IEEE systems under study. For the 68-bus system, as shown in Fig. 16(a), critical features, such as the frequency, voltage magnitude, and active power, are identified. In the analysis of the 25 k bus system, as illustrated in Fig. 16(b), the top features include the voltage angle and magnitude, highlighting the significance of phase relationships and voltage magnitudes in assessing power system stability. Overall, the feature importance analysis underscores that voltage magnitudes, active and reactive power, and frequency metrics are essential for accurate TSA in power systems.

F. MODEL SENSITIVITY TO DATA SIZE

In this section, the model performance is assessed with different sizes of data from the ACTIVSg25k-bus system. It is crucial to consider the size of the dataset when designing and training DL models to ensure efficient training and accurate generalization. Table 9 presents the error metrics of the TCN model across varying data sizes. From Table 9, the model demonstrates significant improvement in precision, F1 score, and accuracy when the percentage of data increases from 10% to 20%. As the data size continues to grow, the improvement in model performance becomes more gradual, with smaller increments in the precision score, F1 score, and accuracy values. It is important to note that the model reaches near-perfect precision, F1 score, and accuracy values when trained with 60% or more of the data. This suggests that the model has a high capacity to learn from the available data and is capable of achieving excellent performance even when trained on a

TABLE 9 Performance Metrics of the TCN-GWO Model Across Varying Data Sizes on the ACTIVSg25 k Bus System

Data size (%)	Samples	Prec (%)	F1 (%)	ACC (%)
10	2400	92.57	96.14	96.09
20	4800	97.68	98.83	98.84
30	7200	96.82	98.38	98.40
40	9600	98.56	99.28	99.29
50	12 000	99.10	99.55	99.56
60	14 400	99.82	99.91	99.91
70	16 800	99.10	99.55	99.56
80	19 200	99.28	99.64	99.64
90	21 600	99.64	99.82	99.82
100	24 004	100.00	99.91	99.91

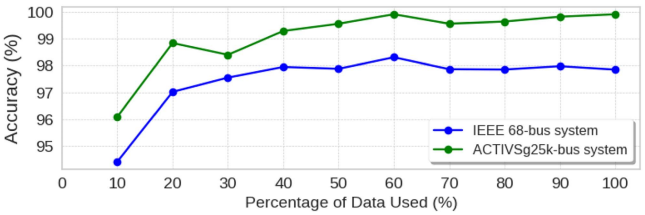

FIGURE 17. Impact of the data completeness on accuracy for the IEEE bus systems using the TCN-GWO model.

relatively smaller proportion of the dataset. Fig. 17 shows the accuracy of the TCN model trained on the IEEE 68k-bus system and the ACTIVSg25k-bus system—as a function of the percentage of data used for training. According to Fig. 17, both systems show an increase in accuracy as more data are used, which is typical because more data generally provide a model with more information to learn from, potentially improving its predictive performance. According to the figure, the IEEE 68k-bus system starts at a lower accuracy with 10% of the data used but shows a significant increase as more data are introduced, reaching its peak at around 40%. It then maintains a relatively stable accuracy despite further increases in data percentage. For the ACTIVSg25k-bus system, the TCN starts with a higher initial accuracy at 10% data usage compared to the 68k-bus system. It increases to its highest point at around 30%, and, similar to the 68k-bus system, it plateaus with little to no increase in accuracy with more data. The plateauing of accuracy for both systems suggests that beyond a certain point, adding more training data does not necessarily lead to significant performance gains, which might indicate that the models have reached their learning capacity or that the additional data do not add new information to further refine the model's understanding. Fig. 18 illustrates the computational efficiency of the TCN-GWO model.

According to Fig. 18(a), as the percentage of training data increases, the TrT exhibits a general upward trend, albeit with some variability. This suggests that more data typically require longer to process during training, which is expected. Regarding Fig. 18(b), the inference time does not show a consistent trend as the training data percentage changes. The

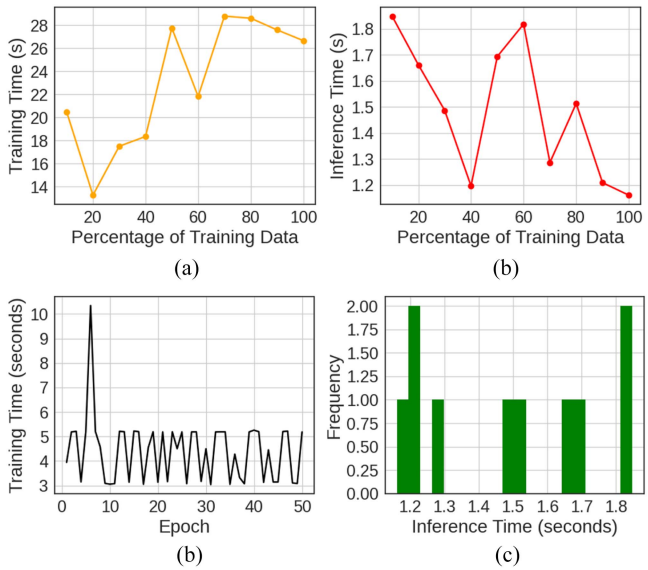

FIGURE 18. Computational efficiency analysis of the TCN-GWO model: (a) TrT versus percentage of training data, (b) inference time versus percentage of training data, (c) TrT per epoch, and (d) inference time distribution, tested on ACTIVSg25-k bus system.

variations are notable and suggest that the relationship between the amount of training data and inference time is not linear or direct. According to Fig. 18(c), the TrT per epoch fluctuates significantly, which may indicate changes in computational load, variations in convergence speed across epochs, or other processing tasks occurring in the background. The downward trend at the beginning might suggests an initial adjustment period for the model, while the following fluctuations indicate that the model training is not entirely stable across epochs. According to Fig. 18(d), the histogram displays the frequency of different inference times recorded. The concentration of inference times around specific intervals indicates the common duration for the model to make predictions on new data. Notably, these results pave the way for exploring deeper aspects of the model's operational envelope.

To build upon this work, the optimized TCN model offers several advantages, including improved accuracy under N-1 contingencies, high computational efficiency compared to RNN-based models, and resilience against PMU data noise, making it suitable for real-time TSA. Nonetheless, two limitations warrant attention: the model may need enhanced interpretability, and it may face challenges in identifying rare transient events and adapting to topological changes in the electric grid without retraining.

VI. CONCLUSION

This article developed an innovative method for transient stability status prediction. The model utilizes a feature selection methodology that undergoes a high feature–feature correlation elimination, followed by a feature ranking. Finally, a forward feature selection is employed while considering the best-performing features. In addition, TCN-based GWO is examined for TSA of power systems. The developed TCN model was successfully implemented on the IEEE 68-bus system and the synthetic 25k-bus Northeastern United States system. The performance of the proposed model is evaluated and compared with other approaches. The various studies performed in this article reveals that inaccuracies from faulty measurements present a greater challenge in predicting transient stability status compared to instances of missing PMU measurements. Further, the model's scalability and effectiveness remain intact, even when the system is scaled up from 68 buses to 25 000 buses. This scalability underscores the model's robustness and adaptability to varying system complexities. In addition, the findings suggest that prediction accuracy improves with larger datasets, indicating the importance of data volume in enhancing the learning process. Overall, the study underscores the model's resilience to data quality issues and its capacity to handle diverse system sizes effectively.

Compared to existing approaches, the proposed model has superior performance in terms of error metrics. Nevertheless, the TCN model has not been tested on unseen faults that have not been included in the training dataset. Therefore, future work will consider fusing the optimized TCN with graph neural networks to inherently recognize patterns within both the temporal sequence of events and the complex interconnectivity of the power grid topology, thus enhancing the classification of rare transient events. Future work will involve leveraging Big Data platforms to improve the model's effectiveness in TSA. In addition, extending this work to address the recently emerging stability issues, such as resonance and converter-driven stability, due to the growing integration of power electronics-dominated grids, represents a meaningful direction.

ACKNOWLEDGMENT

The authors would like to thank the project Responsive Research Seed Grant (RRSG5) and Research Impact Initiative (SP6) for supporting this research work.

REFERENCES

[1] N. Hatziargyriou et al., "Definition and classification of power system stability revisited & extended," *IEEE Trans. Power Syst.*, vol. 36, no. 4, pp. 3271–3281, Jul. 2021.

[2] F. Chang, X. Cui, M. Wang, and W. Su, "Potential-based large-signal stability analysis in DC power grids with multiple constant power loads," *IEEE Open Access J. Power Energy*, vol. 9, pp. 16–28, 2021.

[3] Y. Chen, S. M. Mazhari, C. Chung, and S. O. Faried, "A preventive dispatching method for high wind power-integrated electrical systems considering probabilistic transient stability constraints," *IEEE Open Access J. Power Energy*, vol. 8, pp. 472–483, 2021.

[4] A. Khan, M. Hosseinzadehtaher, M. B. Shadmand, S. Bayhan, and H. Abu-Rub, "On the stability of the power electronics-dominated grid: A new energy paradigm," *IEEE Ind. Electron. Mag.*, vol. 14, no. 4, pp. 65–78, Dec. 2020.

[5] A. R. Sobbouhi and A. Vahedi, "Transient stability prediction of power system; a review on methods, classification and considerations," *Electric Power Syst. Res.*, vol. 190, 2021, Art. no. 106853.

[6] H. Silva-Saravia, H. Pulgar-Painemal, D. A. Schoenwald, and W. Ju, "Adaptive coordination of damping controllers for enhanced power system stability," *IEEE Open Access J. Power Energy*, vol. 7, pp. 265–275, 2020.

[7] K. Ye, J. Zhao, N. Duan, and D. A. Maldonado, "Stochastic power system dynamic simulation and stability assessment considering dynamics from correlated loads and PVs," *IEEE Trans. Ind. Appl.*, vol. 58, no. 6, pp. 7764–7775, Nov./Dec. 2022.

[8] S. Konstantinopoulos and J. H. Chow, "Active power control of DFIG wind turbines for transient stability enhancement," *IEEE Open Access J. Power Energy*, vol. 10, pp. 208–221, 2022.

[9] L. Zhu, W. Wen, J. Li, and Y. Hu, "Integrated data-driven power system transient stability monitoring and enhancement," *IEEE Trans. Power Syst.*, vol. 39, no. 1, pp. 1797–1809, Jan. 2024.

[10] C. Li, H.-D. Chiang, and Z. Du, "Network-preserving sensitivity-based generation rescheduling for suppressing power system oscillations," *IEEE Trans. Power Syst.*, vol. 32, no. 5, pp. 3824–3832, Sep. 2017.

[11] Z. Wang, X. Song, H. Xin, D. Gan, and K. P. Wong, "Risk-based coordination of generation rescheduling and load shedding for transient stability enhancement," *IEEE Trans. Power Syst.*, vol. 28, no. 4, pp. 4674–4682, 2013.

[12] X. Zhou et al., "Transient stability assessment based on gated graph neural network with imbalanced data in internet of energy," *IEEE Internet Things J.*, vol. 9, no. 12, pp. 9320–9331, Jun. 2022.

[13] R. Yadav, S. Raj, and A. K. Pradhan, "Real-time event classification in power system with renewables using kernel density estimation and deep neural network," *IEEE Trans. Smart Grid*, vol. 10, no. 6, pp. 6849–6859, Nov. 2019.

[14] R. Yan, G. Geng, Q. Jiang, and Y. Li, "Fast transient stability batch assessment using cascaded convolutional neural networks," *IEEE Trans. Power Syst.*, vol. 34, no. 4, pp. 2802–2813, Jul. 2019.

[15] F. Pan et al., "Stacked-GRU based power system transient stability assessment method," *Algorithms*, vol. 11, no. 8, 2018, Art. no. 121.

[16] X. Li, C. Liu, P. Guo, S. Liu, and J. Ning, "Deep learning-based transient stability assessment framework for large-scale modern power system," *Int. J. Elect. Power Energy Syst.*, vol. 139, 2022, Art. no. 108010.

[17] B. Tan, J. Yang, Y. Tang, S. Jiang, P. Xie, and W. Yuan, "A deep imbalanced learning framework for transient stability assessment of power system," *IEEE Access*, vol. 7, pp. 81759–81769, 2019.

[18] Y. Ouyang and H. Wang, "Adaptive denoising combined model with SDAE for transient stability assessment," *Electric Power Syst. Res.*, vol. 214, 2023, Art. no. 108948.

[19] S. Wu, L. Zheng, W. Hu, R. Yu, and B. Liu, "Improved deep belief network and model interpretation method for power system transient stability assessment," *J. Modern Power Syst. Clean Energy*, vol. 8, no. 1, pp. 27–37, 2020.

[20] Y. Zhou, Q. Guo, H. Sun, Z. Yu, J. Wu, and L. Hao, "A novel data-driven approach for transient stability prediction of power systems considering the operational variability," *Int. J. Elect. Power Energy Syst.*, vol. 107, pp. 379–394, 2019. [Online]. Available: https://www.sciencedirect.com/science/article/pii/S0142061518319914

[21] A. Bashiri Mosavi, A. Amiri, and H. Hosseini, "A learning framework for size and type independent transient stability prediction of power system using twin convolutional support vector machine," *IEEE Access*, vol. 6, pp. 69937–69947, 2018.

[22] J.-M. H. Arteaga, F. Hancharou, F. Thams, and S. Chatzivasileiadis, "Deep learning for power system security assessment," in *Proc. IEEE Milan PowerTech*, 2019, pp. 1–6.

[23] R. Zhang, J. Wu, Y. Xu, B. Li, and M. Shao, "A hierarchical self-adaptive method for post-disturbance transient stability assessment of power systems using an integrated CNN-based ensemble classifier," *Energies*, vol. 12, no. 17, p. 3217, 2019. [Online]. Available: https://www.mdpi.com/1996-1073/12/17/3217

[24] B. Li and J. Wu, "Adaptive assessment of power system transient stability based on active transfer learning with deep belief network," *IEEE Trans. Autom. Sci. Eng.*, vol. 20, no. 2, pp. 1047–1058, Apr. 2023.

[25] M. Massaoudi, H. Abu-Rub, S. S. Refaat, M. Trabelsi, I. Chihi, and F. S. Oueslati, "Enhanced deep belief network based on ensemble learning and tree-structured of Parzen estimators: An optimal photovoltaic power forecasting method," *IEEE Access*, vol. 9, pp. 150330–150344, 2021.

[26] J. J. Q. Yu, D. J. Hill, A. Y. S. Lam, J. Gu, and V. O. K. Li, "Intelligent time-adaptive transient stability assessment system," *IEEE Trans. Power Syst.*, vol. 33, no. 1, pp. 1049–1058, Jan. 2018.

[27] L. Zheng, W. Hu, K. Hou, X. Xu, and G. Shao, "Real-time transient stability assessment based on deep recurrent neural network," in *Proc. IEEE Innov. Smart Grid Technol. Asia*, 2017, pp. 1–5.

[28] M. Barati, "Faster than real-time prediction of disruptions in power grids using PMU: Gated recurrent unit approach," in *Proc. IEEE Power Energy Soc. Innov. Smart Grid Technol. Conf.*, 2019, pp. 1–5.

[29] A. Gupta, G. Gurrala, and P. S. Sastry, "Instability prediction in power systems using recurrent neural networks," in *Proc. 26th Int. Joint Conf. Artif. Intell.*, 2017, pp. 1795–1801. [Online]. Available: https://doi.org/10.24963/ijcai.2017/249

[30] I. Kiaei, M. Rostami, and S. Lotfifard, "Robust decentralized control of synchronous generators for improving transient stability of multi-machine power grids," *IEEE Syst. J.*, vol. 15, no. 3, pp. 3470–3479, Sep. 2021.

[31] Y. Zhang and L. Xie, "A transient stability assessment framework in power electronic-interfaced distribution systems," *IEEE Trans. Power Syst.*, vol. 31, no. 6, pp. 5106–5114, Nov. 2016.

[32] K. Ye, J. Zhao, H. Li, and M. Gu, "A high computationally efficient parallel partial Gaussian process for large-scale power system probabilistic transient stability assessment," *IEEE Trans. Power Syst.*, vol. 39, no. 2, pp. 4650–4660, Mar. 2024.

[33] M. Shahriyari, H. Khoshkhoo, and J. M. Guerrero, "A novel fast transient stability assessment of power systems using fault-on trajectory," *IEEE Syst. J.*, vol. 16, no. 3, pp. 4334–4344, Sep. 2022.

[34] M. Zhang, W. Luan, S. Guo, and P. Wang, "Topology identification method of distribution network based on smart meter measurements," in *Proc. China Int. Conf. Electricity Distrib.*, 2018, pp. 372–376.

[35] S. Vandermeeren, S. Van de Velde, H. Bruneel, and H. Steendam, "A feature ranking and selection algorithm for machine learning-based step counters," *IEEE Sensors J.*, vol. 18, no. 8, pp. 3255–3265, 2018.

[36] M. Massaoudi, S. S. Refaat, I. Chihi, M. Trabelsi, F. S. Oueslati, and H. Abu-Rub, "A novel stacked generalization ensemble-based hybrid LGBM-XGB-MLP model for short-term load forecasting," *Energy*, vol. 214, 2021, Art. no. 118874.

[37] G. Hafeez, K. S. Alimgeer, and I. Khan, "Electric load forecasting based on deep learning and optimized by heuristic algorithm in smart grid," *Appl. Energy*, vol. 269, 2020, Art. no. 114915.

[38] P. Xia et al., "Adaptive feature utilization with separate gating mechanism and global temporal convolutional network for remaining useful life prediction," *IEEE Sensors J.*, vol. 23, no. 18, pp. 21408–21420, Sep. 2023.

[39] S. Bai, J. Z. Kolter, and V. Koltun, "An empirical evaluation of generic convolutional and recurrent networks for sequence modeling," in *Proc. Int. Conf. Learn. Representations Workshop*, 2018, arXiv:1803.01271.

[40] Y. Zhang, Y. Ma, and Y. Liu, "Convolution-bidirectional temporal convolutional network for protein secondary structure prediction," *IEEE Access*, vol. 10, pp. 117469–117476, 2022.

[41] M. Carreras, G. Deriu, L. Raffo, L. Benini, and P. Meloni, "Optimizing temporal convolutional network inference on FPGA-based accelerators," *IEEE Trans. Emerg. Sel. Topics Circuits Syst.*, vol. 10, no. 3, pp. 348–361, Sep. 2020.

[42] S. Mirjalili, S. M. Mirjalili, and A. Lewis, "Grey wolf optimizer," *Adv. Eng. Softw.*, vol. 69, pp. 46–61, 2014.

[43] S. Blanke, "Hyperactive: An optimization and data collection toolbox for convenient and fast prototyping of computationally expensive models.," 2019. [Online]. Available: https://github.com/SimonBlanke

[44] M. E. Eddin et al., "Fine-tuned RNN-based detector for electricity theft attacks in smart grid generation domain," *IEEE Open J. Ind. Electron. Soc.*, vol. 3, pp. 733–750, 2022.

[45] M. Wang and J. V. Milanović, "The impacts of demand side management on combined frequency and angular stability of the power system," *IEEE Trans. Power Syst.*, vol. 38, no. 4, pp. 3775–3786, Jul. 2023.

[46] "ACTIVSg25 k: 25,000 bus synthetic grid on footprint of northeastern United States," Accessed: Sep. 23, 2019. [Online]. Available: http://electricgrids.engr.tamu.edu/electric-grid-test-cases/activsg25k/

[47] S. K. Azman, Y. J. Isbeih, M. S. El Moursi, and K. Elbassioni, "A unified online deep learning prediction model for small signal and transient stability," *IEEE Trans. Power Syst.*, vol. 35, no. 6, pp. 4585–4598, Nov. 2020.

[48] S. M. Mazhari, N. Safari, C. Chung, and I. Kamwa, "A quantile regression-based approach for online probabilistic prediction of unstable groups of coherent generators in power systems," *IEEE Trans. Power Syst.*, vol. 34, no. 3, pp. 2240–2250, May 2019.

[49] A. Hariri and M. Babaie-Zadeh, "Compressive detection of sparse signals in additive white Gaussian noise without signal reconstruction," *Signal Process.*, vol. 131, pp. 376–385, 2017.

[50] "IEEE standard for synchrophasor measurements for power systems," IEEE Standard C37.118.1-2011 (*Revision IEEE Standard C37.118-2005*), pp. 1–61, 2011.
[51] M. Hijazi, P. Dehghanian, and S. Wang, "Transfer learning for transient stability predictions in modern power systems under enduring topological changes," *IEEE Trans. Autom. Sci. Eng.*, early access, pp. 1–15, Jun. 1, 2023.
[52] A. B. Birchfield, T. Xu, K. M. Gegner, K. S. Shetye, and T. J. Overbye, "Grid structural characteristics as validation criteria for synthetic networks," *IEEE Trans. power Syst.*, vol. 32, no. 4, pp. 3258–3265, Jul. 2017.
[53] T. Xu, A. B. Birchfield, and T. J. Overbye, "Modeling, tuning, and validating system dynamics in synthetic electric grids," *IEEE Trans. Power Syst.*, vol. 33, no. 6, pp. 6501–6509, Nov. 2018.
[54] T. Chen et al., "Power system dynamic security region algorithm based on lightGBM and improved SVM," in *Proc. Int. Conf. Power System Technol.*, 2021, pp. 2027–2032.

MOHAMED MASSAOUDI (Member, IEEE) received the Ph.D. degree in electronics engineering from the National Institute of Applied Sciences and Technology (INSAT), University of Carthage, Carthage, Tunisia, in 2022.

He has eight years of hands-on experience in applying data-driven strategies to tackle real-world problems. During his work with Texas A&M University at Qatar, he was the lead author of more than 40 peer-reviewed journals and conference publications, including IEEE OPEN JOURNAL OF INDUSTRY APPLICATIONS and IEEE TRANSACTIONS ON POWER SYSTEMS. He has an H-Index of 13 and his work has been cited more than 800 times. His research interests include machine learning and deep learning techniques for power system stability, power grid partitioning, and cybersecurity.

Dr. Massaoudi was the recipient of the Outstanding Student Research Excellence Award in 2021, the Thomas W. Powell'62 and Powell Industries Inc., Fellowship award in 2024, and the Richard E. Ewing Award for Excellence in 2024 for his research contributions.

TASSNEEM ZAMZAM received the B.Sc. (Hons.) and M.Sc. degrees in electrical engineering from Qatar University, Doha, Qatar, in 2018 and 2021, respectively. She is currently working toward the Ph.D. degree in electrical engineering with Texas A&M University, College Station, TX, USA.

From 2018 to 2022, she was a Research Assistant with the Electrical Engineering Department, Qatar University. Her research interests include grid stability, reinforcement learning, distributed energy resources, and smart grid.

MAYMOUNA EZ EDDIN received the B.Sc. degree in electrical engineering from Qatar University, Doha, Qatar, in 2020, and the M.Sc. degree in data science and engineering from Hamad Bin Khalifa University, Doha, in 2022. She is currently working toward the Ph.D. degree in electrical and computer engineering with Texas A&M University, College Station, TX, USA.

From 2020 to 2022, she was a Research Assistant with the Qatar University Machine Learning Group. She is currently an Associate Research Assistant with Texas A&M University at Qatar, Doha. Her research interests include the application of deep learning and machine learning in smart grid security, and healthcare.

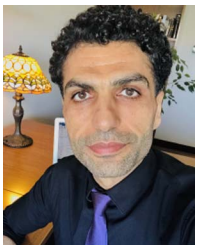

ALI GHRAYEB (Fellow, IEEE) received the Ph.D. degree in electrical engineering from The University of Arizona, Tucson, AZ, USA, in 2000.

He is currently a Professor with the Department of Electrical and Computer Engineering, Texas A&M University at Qatar, Doha, Qatar. Prior to his current position, he was a tenured Professor with the Electrical and Computer Engineering Department, Concordia University, Montreal, QC, Canada. He has coauthored two books and authored or coauthored more than 250 journal and conference papers. His research interests include wireless and mobile communications, physical layer security, massive MIMO, visible light communications, smart grid, artificial intelligence, and machine learning.

Dr. Ghrayeb was an Instructor or Co-Instructor in many technical tutorials at several major IEEE conferences. He was the Executive Chair of the 2016 IEEE WCNC Conference. He was the Member of the IEEE ComSoc Conferences Council, IEEE GITC Committee, and IEEE WCNC Steering Committee. He was in different editorial capacities on a number of IEEE transactions journals. He is currently with the IEEE ComSoc Awards Committee.

HAITHAM ABU-RUB (Fellow, IEEE) received the first Ph.D. degree in electrical engineering from the Technical University of Gdansk, Gdansk, Poland, in 1995, and the second Ph.D. degree in humanities from Gdansk University, Gdansk, in 2004.

He has worked with many universities in many countries, including Poland, Palestine, USA, Germany, and Qatar. Since 2006, he has been with Texas A&M University at Qatar, Doha, Qatar, where for five years, he was the Chair of the Electrical and Computer Engineering Program, and is currently the Managing Director with Smart Grid Center. He has authored or coauthored more than 600 journal and conference papers, five books, and six book chapters. He has supervised many research projects on smart grid, power electronics converters, and renewable energy systems. His research interests include electric drives, power electronic converters, renewable energy, and smart grid.

Dr. Abu-Rub was the recipient of many prestigious national and international awards and recognitions, such as the American Fulbright Scholarship and the German Alexander von Humboldt Fellowship. He is the Coeditor-in-Chief for IEEE TRANSACTIONS ON INDUSTRIAL ELECTRONICS.

SHADY S. REFAAT (Senior Member, IEEE) received the B.A.Sc., M.A.Sc., and Ph.D. degrees in electrical engineering from Cairo University, Giza, Egypt, in 2002, 2007, and 2013, respectively.

He was with the industry for more than 12 years as Engineering Team Leader, Senior Electrical Engineer, and Electrical Design Engineer on various electrical engineering projects. He was an Associate Research Scientist with the Department of Electrical and Computer Engineering, Texas A&M University at Qatar, Doha, Qatar, for more than 11 years. He is currently a Senior Lecturer with the University of Hertfordshire, Hatfield, U.K. Also, he has participated in and led several scientific projects in the last nine years. He has successfully realized many potential research projects. He has authored or coauthored more than 178 journal and conference articles, one patent, and one book. His research interests include electrical machines, power systems, smart grid, Big Data, energy management systems, reliability of power grids and electric machinery, fault detection, and condition monitoring and development of fault-tolerant systems.

Dr. Refaat is a Member of the Smart Grid Center–Extension in Qatar (SGC-Q) and The Institution of Engineering and Technology (IET).